Modeling-Based Examination of Conducted EMI Emissions from Hard- and Soft-Switching PWM Inverters

Huibin Zhu and Jih-Sheng Lai
Center for Power Electronics Systems
Virginia Polytechnic Institute and State University
Blacksburg, VA 24061-0111

Allen R. Hefner, Jr.
Semiconductor Electronics Division
National Institute of Standards and Technology
Gaithersburg, MD 20899

Yuqing Tang
Ecostar Electric Drive Systems
15001 Commerce Dr., North
Dearborn, MI 48120

Chingchi Chen
Ford Vehicle Electronics Dept.
20000 Rotunda Dr., MD#1170
Dearborn, MI 48124-2053

ABSTRACT—**For the purpose of investigation of electromagnetic interference (EMI) mechanisms in hard- and soft-switching PWM inverters, empirical models and comparative experiments were studied in both time-domain and frequency-domain. Models of the major circuit components including switching devices, passive components and interconnects were obtained with physics-based device modeling and time-domain reflectometry (TDR) for parasitics characterization. The inverter simulation was then constructed using all the empirical models, and the results were compared with those from prototype experiments to examine the significant roles of parasitic elements coupled with device switching dynamics in EMI generations. With separation of common- and differential-mode EMI, the modeling approach is demonstrated to be effective over most of the EMI frequency range and the soft-switching effects on EMI are discussed.**

I. INTRODUCTION

It is typical today that PWM inverters require high-speed switching devices such as the insulated gate bipolar transistor (IGBT) to achieve high performances in dynamic response, efficiency, acoustic noise, size, and weight. However, these fast switching devices generate high voltage slew rate (*dv/dt*) and high common-mode voltage [1-3]. High *dv/dt* can result in premature insulation failure resulting in the failure of inductor, motor, or transformer. High *dv/dt* is also largely responsible for conducted EMI as identified in [4-8].

In recent years, EMI considerations have become increasingly important, as electromagnetic compatibility (EMC) regulations (typically defined from 10 kHz to 30 MHz) have become more stringent. It is commonly realized that high switching *dv/dt* and *di/dt* are the main sources of EMI noise. The higher *dv/dt* or *di/dt* the switching has, the higher EMI emissions. However, a PWM inverter system is very complicated in terms of the power stage (components and their interconnect parasitics), control circuit, and external connections. While some EMI phenomena have been described and some useful conclusions given in recent studies [3-8], the fundamental mechanisms by which EMI noises are excited and propagated have not been sufficiently investigated.

Moreover, it is well known that various soft-switching techniques can significantly reduce the *dv/dt* or *di/dt* as well as switching losses. It is conceivable that the EMI noise generated by a hard-switching PWM inverter could be reduced by soft-switching techniques. However, whether soft switching can improve EMI performance and how the process works has not been adequately addressed and many questions remain on this issue. Therefore, a better understanding of the EMI mechanisms and of the effects of soft-switching techniques on EMI is needed. Computer-based EMI analyzing tools are desirable to aid in this understanding and to facilitate inverter designs for improved EMC performance or for applying cost-effective EMI reduction techniques to existing systems.

In this paper, EMI generation mechanisms in a zero-voltage-transition (ZVT) soft-switching PWM inverter is studied through an empirical modeling approach as a continuation of previous work on hard-switching inverter [9]. An essential part of such an EMI study is the modeling of device switching dynamic behavior and identification and characterization of various inverter parasitic elements. A physics-based IGBT model developed by Hefner [10-11] was used for correct switching waveforms with high-frequency effects such as *dv/dt* and current tailing. The inverter parasitics were characterized with the time-domain reflectometry (TDR) method [12]. The inverter circuit simulation was constructed with all the empirical models included and the results were compared with experiments to examine the significant roles of parasitic elements coupled with device switching dynamics in the EMI excitation and propagation. With separation of common- and differential-mode EMIs, the validity of the modeling approach is verified and the soft-switching effects on EMI are discussed. This discussion is based on simulations as well as experiments on a 50 kW full-bridge IGBT inverter prototype [13].

II. PROTOTYPE INVERTER AND TEST SETUP

In this work, the EMI study was conducted on a full-bridge PWM inverter under hard- and soft-switching

This project was supported by the National Institute of Standards and Technology and by the Ford Motor Company. This work made use of ERC shared facilities supported by the National Science Foundation under award EEC-9731677. Contribution of the National Institute of Standards and Technology is not subject to copyright.

0-7803-5589-X/99/$10.00 © 1999 IEEE

operations. The results of this EMI study can be extended to a three-phase inverter, as both should possess the same basic mechanisms in EMI excitation and propagation.

Figure 1 shows the circuit of a full-bridge IGBT based inverter with the dashed lines indicating the auxiliary circuit added to achieve zero-voltage turn-on condition for the main IGBT switches [13]. The prototype PWM inverter was designed to have a rating of 50 kW at 300 V dc bus voltage and to be operated at 20-kHz switching frequency. The main switch pairs, S_1-S_2 and S_3-S_4, are half-bridge IGBT modules rated at 600V/400A. The auxiliary circuit consists of resonant capacitors (C_1~C_4), resonant inductor (L_r), two switches (SA_1 and SA_2), and two diodes (DA_1 and DA_2). The two diodes DA_1 and DA_2 are ultra fast soft recovery diodes and the auxiliary switches SA_1 and SA_2 are two IGBT's in one half-bridge module. One feature of the ZVT circuit is that the current rating required for the auxiliary switches is only a fraction of that required for the main switches.

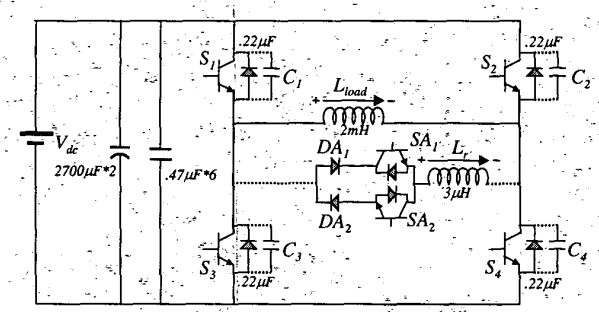

Fig. 1 A ZVT soft-switching full-bridge inverter.

In the inverter operation, each pair of the main switches (i.e., S_1 and S_4, or S_2 and S_3) are turned on or off simultaneously, as controlled by a PWM signal generated by comparing a sinusoidal signal with a 20-kHz triangular signal. The resonant capacitors function as snubbers and slow down the rising rate of the voltage across the main switches at their turn-off. Before the main switches turn on, a corresponding auxiliary switch turns on and the resonant inductor is charged with an adequate current. Next, the resonance between the resonant inductor and the capacitors begins and it brings the voltage across the main switch to zero before the switch turns on. Thus, the zero-voltage condition can be achieved and the reverse recovery problem of the anti-parallel diode of the main switch can be alleviated.

Because EMI is closely related to circuit layout and interconnections, a custom-made laminated bus bar is adopted to enable a compact layout and reduce interconnect parasitics. Two bulk capacitors at 2700 μF each were connected to the two ends of the laminated bus bar. Six high-frequency polypropylene capacitors were mounted directly on top of the bus bar to reduce the interconnect inductance. The inverter layout was carefully designed and only a minimal change of connections was needed between hard-switching and soft-switching operation, so that the inverter structure and the interconnects remain the same for the comparison.

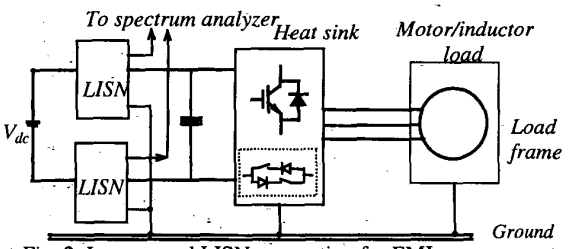

Fig. 2. Inverter and LISN connection for EMI measurement.

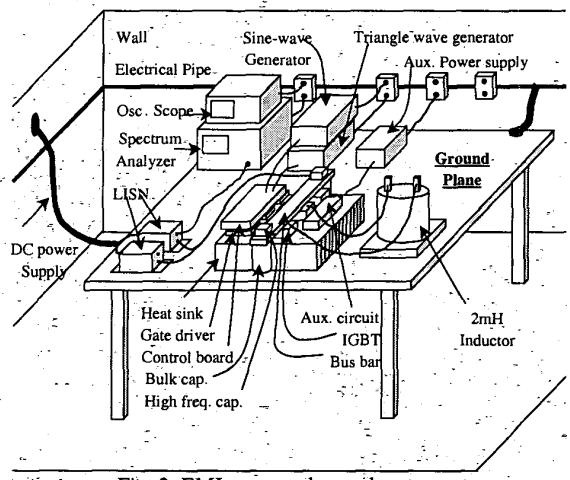

Fig. 3. EMI room and complete test setup.

The connection of the prototype inverter with the load and two line-impedance-stabilizing-networks (LISNs) is shown in Fig. 2. As required by EMC regulations, a large ground reference plane was used as the earth ground. Each LISN provides 50-Ω impedance to the system under test. It also prevents the noise in the source from entering the system under test. For safety reasons, the load frame and the inverter heatsink were grounded, as indicated by the connections to the ground reference plane in Fig. 2. Conducted EMI measurements were made by observing the voltage developed across the defined LISN impedance with a spectrum analyzer. With this configuration, the total EMI noise can be measured on either of the two LISN impedances, while CM or DM EMIs can be separated by taking the sum or difference, respectively, of the signals picked up by the two LISNs.

The EMI room and complete test setup is shown in Fig. 3. Because the purpose of the study is to analyze the source and propagation mechanism of EMI, the setup tends to allow ease of operation, but not to fully comply with EMC regulations. The background noise generated by the instruments, before starting the inverter, was noted and recorded for reference purpose.

III. Inverter Modeling

For the purpose of examining EMI generation, accurate models of device and component in the circuit along with good simulation tools are desirable. Models required in the

simulation include those for the power devices, parasitics of passive component, cables and interconnects, stray capacitors, and ground coupling.

A. Device Model

For an accurate power semiconductor device model, several effects need to be considered with high priority, because they dominate the high-frequency switching characteristics. These important effects include resistivity modulation, charge storage, MOS capacitances, electrothermal interaction, and breakdown phenomenon. Special challenges in developing such models for circuit simulation arise from the need to simultaneously fulfill contradicting requirements including high quantitative accuracy, low demand for computation power, and low demand for physical, structural model parameters.

Recently, a physics-based IGBT model has been developed for the first time by Hefner and has become available in the Saber simulator [10-11]. The IGBT modeling work also provides a detailed parameter extraction method. Such an advanced IGBT model with high-frequency switching characteristics is necessary to obtain correct switching waveforms such as *dv/dt* and current tailing. The model parameters of the IGBT device used in the prototype inverters are extracted with experiments.

Various parasitics exist inside an IGBT module. The authors have proposed the use of TDR measurement for characterization of lead and interconnect parasitics in [12]. With the TDR method, the lead and interconnect inductances in the IGBT module can be measured without intruding the device. In addition, there are parasitic capacitances between IGBT collectors and the module metal baseplate. These capacitances cause a high-frequency leakage current to flow to the metal baseplate that is connected to the heatsink. The heatsink is normally grounded for safety reasons. The IGBT devices are mounted on the metal base plate with a thin electrical insulating material sandwiched in between. To make the thermal resistance small, the insulating layer is normally made as thin as possible, but the stray capacitance between the collector and the base plate tends to be large. With inclusion of interconnect inductance and the stray capacitance, the complete IGBT module equivalent circuit can be obtained as reported in [9,12].

B. Parasitic Models of Bus Bar and Bulk Capacitor

The custom-designed bus bar and the dc bulk capacitor used in the prototype inverter are characterized using the TDR method [12]. The bus bar is used to connect the dc power source to the three IGBT inverter output legs. The bus bar has three sets of bushings in the middle for connection to the IGBT modules, which divide the bus bar into four equal-length sections, and thus the bus bar behaves like a transmission line with a characteristic impedance and a total time delay. As shown in [12], the transmission line model can be partitioned into four equal segments and approximated as four *LC* filters in series.

For capacitors, the parasitic component that affects EMI the most is the equivalent series inductance (ESL) and the ESR. With the TDR measurement result, the ESL of a 450 V, 2700 μF electrolytic capacitor was evaluated [12].

IV. Time Domain Comparative Study

The EMI production mechanism includes noise sources and noise paths. The noise source is related to the voltage and current rates of change, i.e., *dv/dt* and *di/dt*. These rates of change can be observed in time-domain study. With the inclusion of major parasitic components and the use of a physics-based device model, the simulated and experimental IGBT turn-on and turn-off voltage and current waveforms under hard switching are shown in Figs. 4 and 5, respectively. The ZVT soft-switching turn-on waveforms are shown in Fig. 6. It can be seen in this figure that the gate signal *Vg* is applied after *Vce* drops to zero.

Because parasitics in the sensor connections and instrumentation probes were not included in the simulation model, some high-frequency oscillations shown in the experimental waveforms were not quite predicted in the simulation. However, both turn-on and turn-off voltage and current rates of change are well matched with the computer simulation. Although the additional parasitic components can alter the frequency-domain characteristics, their energy level is low, and it was better to neglect them for this study to avoid unnecessary complexity and difficulty of convergence in the simulation process.

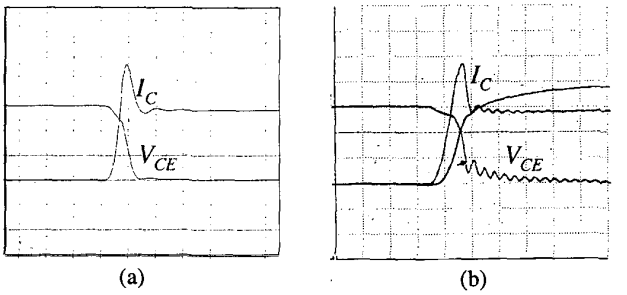

Fig. 4. IGBT hard-switching turn-on waveforms (a) simulation, (b) experiment with V_{CE}:100V/div, I_C:40A/div, and *Time*:200 ns/div.

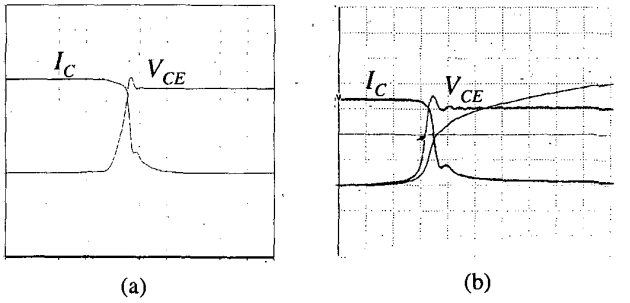

Fig. 5. IGBT hard-switching turn-off waveforms (a) simulation, (b) experiment with V_{CE}:100V/div, I_C:40A/div, and *Time*:200 ns/div.

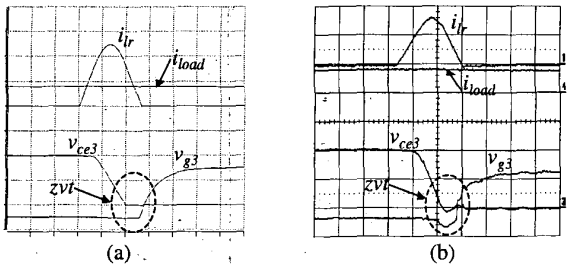

Fig. 6. IGBT ZVT turn-on waveforms (a) simulation, (b) experiment with V_{CE}:100V/div, I:40A/div, and *Time*:1μs/div.

V. Frequency Domain Comparative Study

The inverter operation was simulated to obtain its EMI spectra using the developed circuit model with major parasitic inductances and capacitances in device modules, passive components, leads, and interconnects. The inverter simulation was in time domain, and the EMI spectra were then calculated from the time-domain noise voltage picked up by the LISNs using fast Fourier transformation (FFT). To verify the validity of the inverter model, a comparative study was performed between simulations and experiments with the inverter operating at the same conditions.

Conducted EMI performance, defined from 10 kHz and 30 MHz, is normally examined over two different frequency ranges: 1)low frequency range (from 10 kHz to 150 kHz), and 2)high frequency range (from 150 kHz to 30 MHz). The comparisons of the inverter EMI spectra under hard switching operation are conducted between simulations and experiments and the results reported in the previous paper [12]. Based on the comparative EMI waveforms in [12], the observation can be made that the simulation and experimental results match well in the low-frequency range. However, for the high-frequency range, only a fair matching (less than 10-dB difference) can be seen at the frequencies up to 10 MHz, and a mismatching at the frequencies higher than 10 MHz.

For the sake of the discussions later in this section on the comparison of EMI spectra between hard switching and soft switching, especially in the high-frequency range, it is convenient to repeat the hard-switching EMI waveforms here. Due to space limitation, only the simulated EMI spectra with hard switching for the high-frequency range are repeated, as shown in Fig. 7 where the total noise, DM and CM noise are displayed separately.

For the inverter's soft-switching operation, Figs. 8 and 9 show the comparison of the low-frequency EMI noise spectra between simulation and experimental results, and Figs. 10 and 11 show that of the high-frequency range, with separation of the CM and DM noises from the total noises.

Figs. 8(a), 8(b), and 8(c) are the simulated total, DM, and CM EMI spectra, respectively; while Figs. 9(a), 9(b) and 9(c) are the experimental counterparts. As shown in Figs. 8 and 9, the EMI noises in the low frequency range have high peaks at the multiples of the 20-kHz (i.e., the switching frequency), and the DM noise is the dominant component as compared to

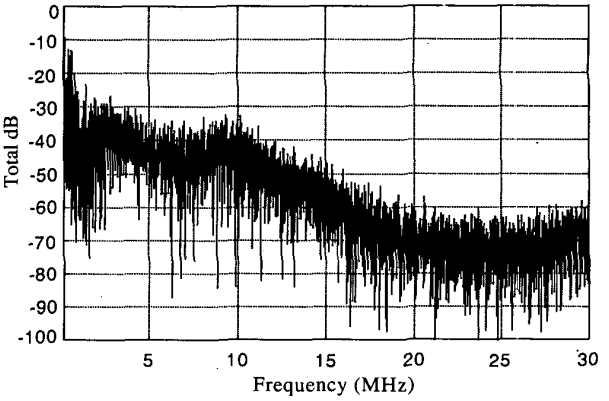

(a) Simulated total EMI spectrum in the high-frequency range.

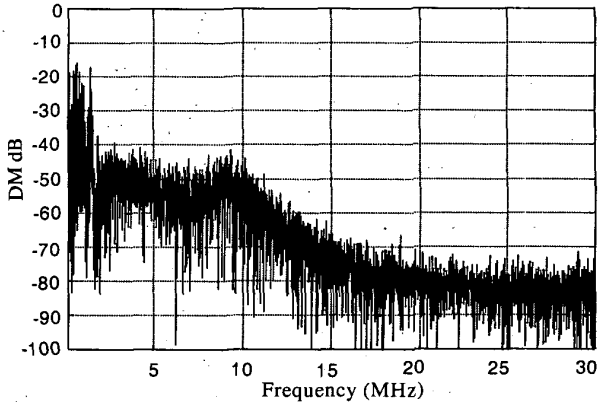

(b) Simulated DM EMI spectrum in the high-frequency range.

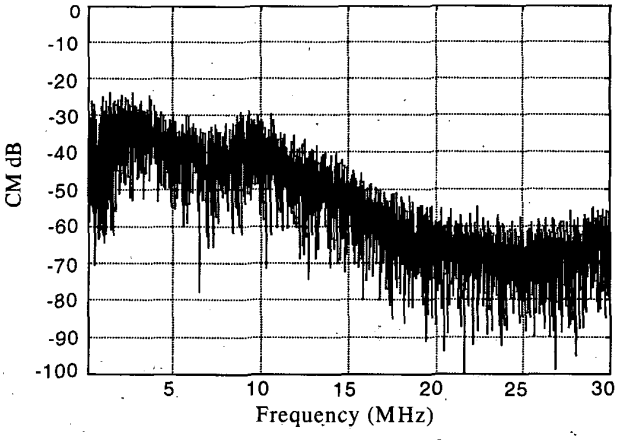

(c) Simulated CM EMI spectrum in the high-frequency range.

Fig. 7. Simulated EMI noise spectra in the high-frequency range for hard switching of the 50 kW IGBT inverter.

the CM noise. From this low-frequency comparison, it can be seen that the simulation and experimental results match well at the frequencies of the multiple peaks. At the frequencies in between those multiple peaks, they do not match quite well due to the fact that the much smaller value

at those frequencies causes relatively much higher errors in the calculations.

Moreover, only the EMI spectra at the peaks are important, because those in between the peaks are too small to be of interest.

For the EMI comparison in the high frequency range, the simulation results of the total, DM, and CM noises are shown in Figs. 10(a), 10(b), and 10(c), respectively; while the experimental counterparts are shown in Figs. 11(a), 11(b), and 11(c), respectively. The inverter operating conditions for the shown EMI spectra are the same with a 300-V source voltage and a 50-A *RMS* load current with a 100-Hz fundamental frequency.

By comparing the simulated total EMI shown in Fig. 10(a) with the experimental one in Fig. 11(a), a fair matching (about 10-dB difference) can be observed at the frequencies lower than 10 MHz. At frequencies higher than 10 MHz, the waveform matching is worse.

From the simulated DM EMI in Fig. 10(b) vs. the experimental one in Figs. 11(b), one can see that the waveform matching is acceptable with less than 10-dB error at the frequencies lower than 6 MHz and the error is less at the higher frequencies.

For the case of CM noise with Figs. 10(c) vs. 11(c), the simulated EMI match fairly well with the experiment in the most of the frequency range. However, in the frequency range from 5 MHz to 15 MHz, the mismatching error is more than 10-dB.

The path of DM EMI consists mainly of the parasitic inductance of device, bulk capacitor, and interconnects. The DM noise current flows through the inductor windings, through the winding capacitance of the inductor, and back to the power mains via the dc bus. It should be noticed that in the comparison between Figs. 10(b) and 11(b), the DM noise spectra match quite well between simulation and experiment. In other words, the inclusion of all the parasitic components in the DM path is valid for the entire low-frequency range and most of the high-frequency range. The IGBT model, which affects the effectiveness of the noise source, is also valid to a large extent.

However, because the matching is not good, the modeling of the CM EMI is not sufficient. The CM noise current flows through the stray capacitance of the load inductor to the inductor frame and back to the source via the power mains. The common-mode current also flows through the stray capacitance between the IGBT collector and the module's baseplate that is normally grounded through the heatsink.

The mismatching of high-frequency EMI spectra between simulations and experiments can be considered as follows:

(1) The gate drive and gate drive power supply noises are not included. These noises contain mainly high frequency DM and CM noises [8].

(2) The CM path parasitic components are not included sufficiently. In the simulation, the only major CM path that is included is the parasitic capacitance between IGBT and heatsink. Other CM paths created by load, power supply transformers, opto-couplers, control circuit switchings, etc. were not included.

(3) The background EMI noises from instrumentation and their associated power supplies were neglected.

(4) The sampling and computational methods for spectrum analysis are different between simulation and experiment. The simulation takes limited sampling data and performs FFT for only one fundamental cycle. However, the experimental results contain a significant amount of data, and its spectra are obtained from quasi-peak mode analysis.

(5) The implementation of the auxiliary switch was different in simulation than that used in the experiments. The auxiliary switch used in the simulation was an IGBT device model, while the devices in the experiments were MOS-controlled thyristors (MCT's).

As indicated by both simulation and experiment results, the CM noise is the dominant part compared to the DM noise with soft-switching operation, especially at frequencies higher than 10 MHz, as is the case with hard switching operation [9].

By comparing the hard-switching results shown in [9] to the soft-switching counterparts shown in Fig. 9 through Fig. 11, it was found that the soft-switching technique contributes significantly in reducing the DM EMI (especially in the frequency range higher than 1 MHz). However, the soft-switching technique has much smaller affects on CM EMI. An improvement on the total EMI with soft-switching operation was also noticed.

Because DM noise is related to high *di/dt* and the high *di/dt* caused by the reverse recovery of the anti-parallel diode of the main switches is largely reduced by the ZVT soft switching, the soft-switching technique helps reduce DM noise.

One may expect that with a reduced *dv/dt* across the main IGBT's due to the snubber capacitors in soft switching, the CM EMI should also be proportionally reduced. However, despite the fact that the main switches' *dv/dt* is reduced, the auxiliary branch is doing hard switching at turn-on instead of ZVT operation and has excessive ringing at turn-off as found in the experiments. The ringing is due to reverse recovery problems of the auxiliary branch diodes even under zero-current turn-off condition. The ringing generates large voltage spike with high *dv/dt* across the auxiliary switches and thus causes undesirable CM current flowing through the stray capacitance of the auxiliary branch. This is an important issue that needs to be dealt with.

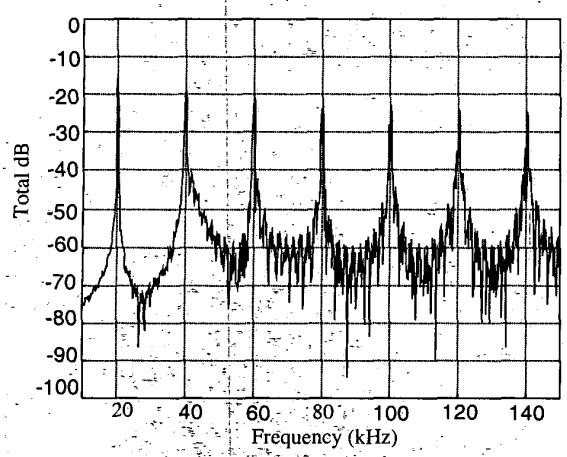

(a) Simulated total spectrum in the low-frequency range.

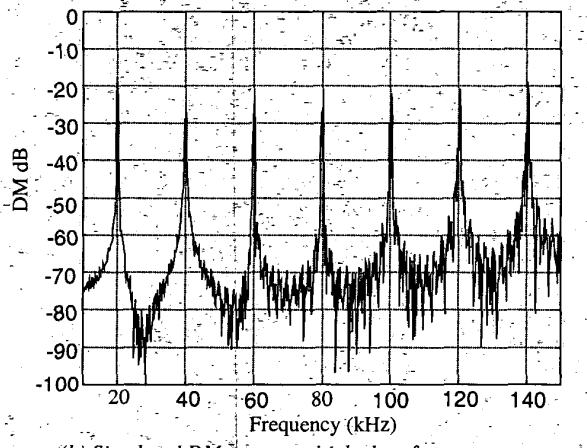

(b) Simulated DM spectrum in the low-frequency range.

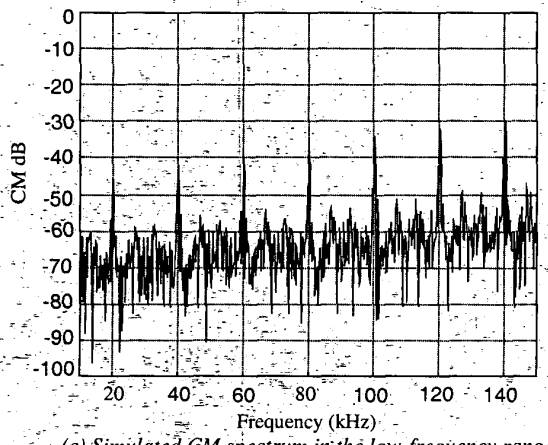

(c) Simulated CM spectrum in the low-frequency range.

Fig. 8. Simulated EMI spectra in the low-frequency range for soft-switching of the 50 kW IGBT inverter.

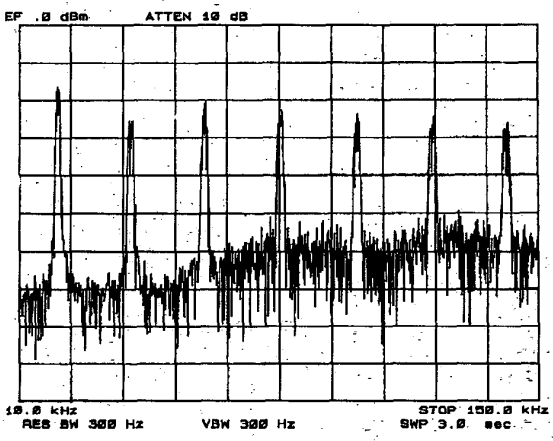

(a) Experimental total spectrum in the low-frequency range.

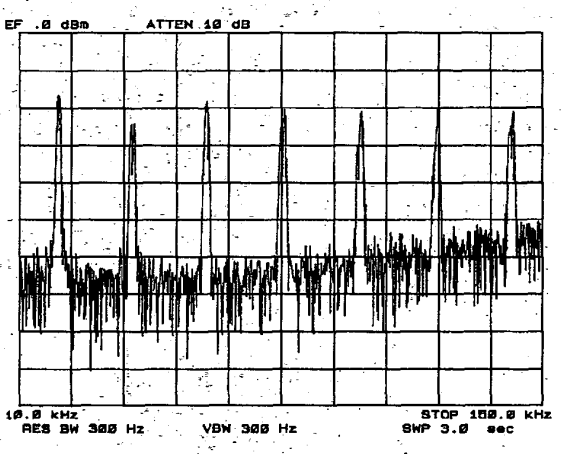

(b) Experimental DM spectrum in the low-frequency range.

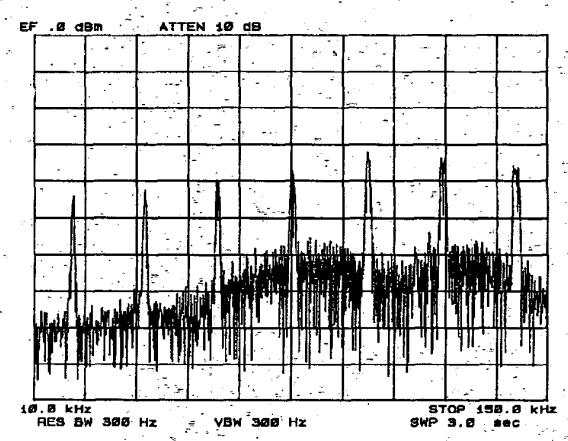

(c) Experimental CM spectrum in the low-frequency range.

Fig. 9. Experimental EMI spectra in the low-frequency range for soft switching of the 50 kW IGBT inverter.

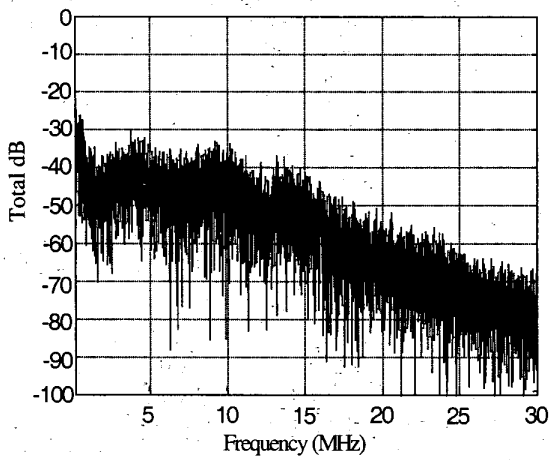

(a) Simulated total spectrum in the high-frequency range.

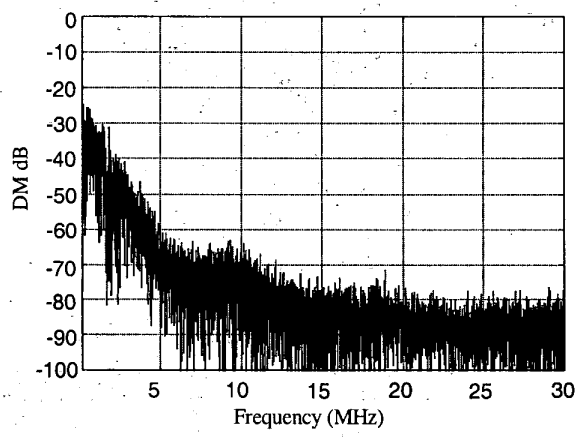

(b) Simulated DM spectrum in the high-frequency range.

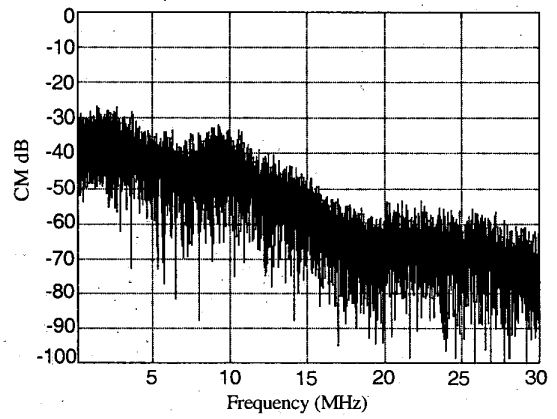

(c) Simulated CM spectrum in the high-frequency range.

Fig. 10. Simulated EMI spectra in the high-frequency range for soft-switching of the 50 kW IGBT inverter.

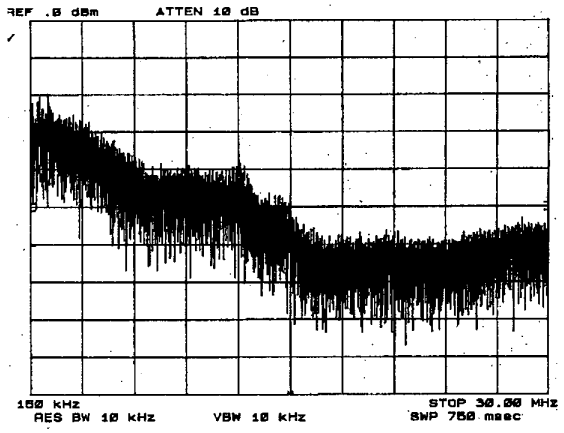

(a) Experimental total spectrum in the high-frequency range.

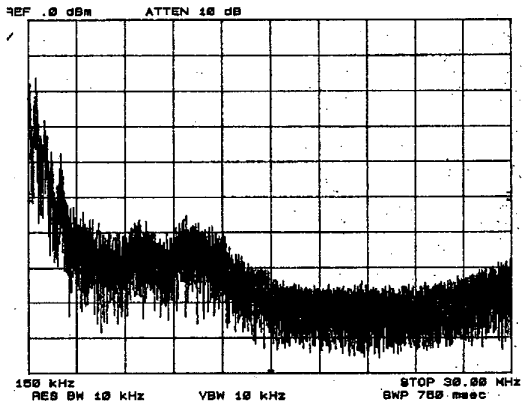

(b) Experimental DM spectrum in the high-frequency range.

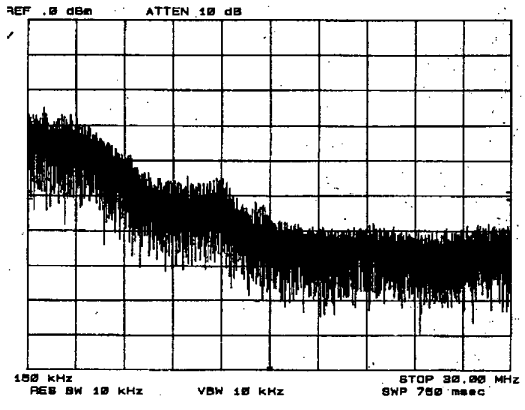

(c) Experimental CM spectrum in the high-frequency range.

Fig. 11. Experimental EMI noise spectra in the high-frequency range for soft-switching of the 50 kW IGBT inverter.

VI. Conclusion

In this paper, EMI generation mechanisms in PWM inverter was studied through an empirical modeling approach with ZVT soft-switching operation as well as with hard switching operation. The inverter's major parasitics were characterized with the time-domain reflectometry method. A physics-based IGBT model was used in simulation for correct switching dynamic waveforms. The significant roles of parasitic elements coupled with device switching dynamics in EMI excitation and propagation were demonstrated. Also the modeling approach was examined with simulation results compared to actual experiments, and its validity is verified. This new approach of EMI investigation turns out to be effective in the low-frequency range and most part of the high-frequency range. In addition, it is found that the soft-switching technique contributes significantly in reducing the DM and the total EMI (especially in the frequency range higher than 1 MHz), while it has much smaller affects on the CM EMI.

Acknowledgment

The authors would like to thank David Berning, Bruce Shen, and Sebastien Bouche of the National Institute of Standards and Technology for their work on the IGBT model parameter extractions.

References

[1] J. Erdman, R. J. Kerkman, D. Schlegel, et al., "Effect of PWM inverters on AC motor bearing currents and shaft voltages," in *Conf. Rec. of IEEE APEC*, 1995, pp. 24–33.

[2] Von Jouanne, P. Enjeti, et al., "The effects of long motor leads on PWM inverter fed AC motor drive systems," in *Conf. Rec. of IEEE APEC*, 1995, pp. 592–597.

[3] S. Chen, T. A. Lipo, D. Fitzgerald, "Modeling of motor bearing currents in PWM inverter drives," in *Conf. Rec. of IEEE IAS Ann. Mtg.*, 1995, pp. 388–393.

[4] T. Shimizu, G. Kimura, "Analysis of high frequency leakage current caused by parasitic capacitor of the power transistor module," in *Conf., Rec. of IPEC*, 1995, pp. 217–222.

[5] E. Zhong, T. A. Lipo, "Improvements in EMC performance of inverter-fed motor drives," *IEEE Trans. Ind. Appl.*, Dec. 1995, pp. 1247–1256.

[6] L. Ran, S. Gokani, et al., "Conducted electromagnetic emissions in induction motor drive systems Part I: Time domain analysis and identification of dominant modes," *IEEE Trans. Power Electron.*, Sep. 1998, pp. 757–767.

[7] F. Costa, et al., "Influence of the driver circuits in the generation and transmission of EMI in a power converter: effects on its electromagnetic susceptibility," *European Power Electronics Journal*, March 1995, pp. 35–44.

[8] C. Chen, X. Xu, D. M. Divan, "Conductive electromagnetic interference noise evaluation for an actively clamped resonant dc link inverter for electric vehicle traction drive applications," in *Conf. Rec. of IEEE IAS Ann. Mtg.*, 1997, pp. 1550–1557.

[9] H. Zhu, J.-S. Lai, A. R. Hefner, Jr., et al., "Analysis of conducted EMI emissions from PWM inverter based on empirical models and comparative experiments," in *Conf. Rec. of IEEE PESC*, 1999, pp. 1727–1733.

[10] A. R. Hefner, Jr., D. M. Diebolt, "An experimentally verified IGBT model implemented in Saber circuit simulator," *IEEE Trans. Power Electron.*, Sept. 1994, pp. 532–542.

[11] A. R. Hefner, Jr., "A dynamic electrothermal model for the IGBT," *IEEE Trans. Ind. Appl.*, Mar. 1994, pp. 394–405.

[12] H. Zhu, J.-S. Lai, A. R. Hefner, Jr., et al., "Analysis of conducted EMI emissions from PWM inverter based on empirical models and comparative experiments," in *Conf. Rec. of IEEE PESC*, 1999, pp. 1727–1733.

[13] Y. Tang, H. Zhu, J.-S. Lai, et al., "EMI experimental comparison of PWM inverter between hard- and soft-switching techniques," in *Proc. of the IEEE Workshop on Power Electronics in Transportation*, Michigan, October 1998.